

Semi-Microscopical Description of the Scission Configuration in the Cold Fission of ^{252}Cf

Ş. Mişicu^a and P. Quentin^b

^a*National Institute for Physics and Nuclear Engineering, Bucharest-Măgurele, Romania*

^b*Centre d'Etudes Nucléaires de Bordeaux-Gradignan, Université Bordeaux I and IN2P3/CNRS, France*

Abstract

The cold(neutronless) fission of ^{252}Cf is studied in the frame of a molecular model in which the scission configuration is described by two aligned fragments interacting by means of Coulomb (+ nuclear) forces. The study is carried out for different distances between the fragments tips and excitation energies. For a given deformation, the fragment's total energy is computed via the constrained Hartree-Fock + BCS formalism. The total excitation energy present in the fragments is supposed to contribute only to the fragments deformation and the asymptotic value of the kinetic energy is equated to the inter-fragment potential at scission. These two constraints yield not more than one or two fission channels for a fixed tip distance and excitation energy. Discarding those fission channels corresponding to a disequibrated sharing of the excitation energy between the two fragments, we were able to establish the most likely scission configurations for a specified excitation energy.

PACS numbers 21.60.Gx, 21.60.Jz, 24.75.+i, 25.85.Ca

Keywords: Cold Fission; Cluster model; Hartree-Fock approximation;

1 Introduction

In last time a renewed interest in the spontaneous fission (sf) of ^{252}Cf arised in connection with modern experimental techniques, based on large Ge detector arrays, which allow a better determination of the mass, charge and angular momentum content of the fragments[1].

A particular attention has been payed to the limiting case of *cold fission*, when no neutrons are emitted and the energy released in the reaction is converted entirely in the kinetic energy of the fragments. Some features of this process have been very recently explained satisfactory using cluster like models[2,3].

In these models it is assumed that at scission the fragments have very compact shapes, close to the ground state and thus they are carrying very small excitation energy. The scission configuration consists of two co-axial fragments with a certain distance d between their tips. In the model proposed by Gönnerwein et al.[4], the cold fission was studied by determining the distance d_{min} of the closest approach between the two fragments, when the Q -value equals the interaction energy. This model predicted the smallest tip distance (below 3 fm) for fragments, with mass numbers between 138 and 158 and around the double magic ^{132}Sn , emerging in the sf of ^{252}Cf . Small tip distances were interpreted as a sign of cold fission due to the higher interaction energies at scission.

In the past the scission-point model succeeded also to explain roughly some basic observables of low-energy fission. Based on the assumption of statistical equilibrium among the collective degrees of freedom at the scission point, Wilkins et al. [5] calculated the relative probabilities of formation of complementary fission fragment pairs from the relative potential energies of a system of two coaxial, quadrupole deformed liquid drops, with shell corrections taken into account. The distance between their tips, the intrinsic excitation energy and collective temperature were chosen as the free parameters of the model. In this way the general features of the distributions of mass, nuclear charge and kinetic energy in the fission of various nuclides, ranging from Po to Fm were well reproduced. Using similar ideas, Nörenberg[6] computed the level schemes, equilibrium deformations of the fragments, total energies and charge distributions of ^{236}U , $^{240-242}\text{Pu}$ using the BCS wave-function in the description of the ground state.

In this paper we generalize the static scission-point concept of nuclear fission model in such a way that instead of describing the fragments as two deformed nearly touching liquid drops with shell corrections taken into account, we incorporate the fragments shell structure by means of the self-consistent Hartree-Fock(HF) method. For the given binary splitting $^{252}\text{Cf} \rightarrow ^{104}\text{Mo} + ^{148}\text{Ba}$ we first established the equilibrium deformations of the two fragments by seeking the HF minimum and next their total energy for various deformations is computed by constraining their quadrupole moments. The two fragments are considered as coaxial with distance d between their tips.

One of the basic approximation employed in this paper was that the interaction energy at scission is transformed into kinetic energy of the fragments at infinity. Thus, all the excitation energy present in the fissioning system is accounted by the deformation energy. This amounts to neglect that part of the energy released at the descent from saddle to scission which is spent on heat. Thus, our study concerns mainly the low-energy domain of sf including the limiting case of cold fission [4,7].

By using the above mentioned constraints we were able to deduce the possible

shapes of the fragments for various tip distances and total excitation energies E^* .

2 Molecular Model of Low Energy Fission

2.1 Energy Balance

In the sf of ^{252}Cf the fragments are born with a certain deformation and will carry a total excitation energy E^* , gained during the descent from saddle to scission which will be dissipated by means of neutron and gamma emission[8]

$$Q = V_{sciss} + TK E_{pre} + \sum_{1,2} E_{def}(i) + \sum_{1,2} E_{int}(i) \quad (1)$$

where $V_{sciss} = V_{coul} + V_{nucl}$ represents the fragments interaction energy at scission. For V_{coul} we choose the form corresponding to two deformed homogeneously charged nuclei with collinear symmetry axes with a distance R between their centers [9]

$$V_{coul} = \sum_{\lambda_1=0}^{\infty} \sum_{\lambda_2=0}^{\infty} \frac{3}{\hat{\lambda}_1^2(\hat{\lambda}_1^2 + 2)} \frac{3}{\hat{\lambda}_2^2(\hat{\lambda}_2^2 + 2)} \frac{(2\lambda_1 + 2\lambda_2)!}{(2\lambda_1)!(2\lambda_2)!} x_1^{2\lambda_1} x_2^{2\lambda_2} \quad (2)$$

The variables x_1 and x_2 are expressed in terms of the semiaxes a and b

$$x_{1,2} = \frac{a_{1,2}^2 - b_{1,2}^2}{R^2} \quad (3)$$

The above double series is converging for $|x_1| + |x_2| < 1$ and the final result is given, according to [10] :

$$V_{coul} = \frac{3Z_1 Z_2 e^2}{40R^2} \left\{ \frac{1}{x_1^2 x_2^2} (1 + 11x_1^2 + 11x_2^2) + P_x P_y \left[\frac{(1 + x_1 + x_2)^3}{x_1^3 x_2^3} \right. \right. \\ \left. \left. \ln(1 + x_1 + x_2)(1 - 3x_1 - 3x_2 + 12x_1 x_2 - 4x_1^2 - 4x_2^2) \right] \right\} \quad (4)$$

For the attractive nuclear potential we choose the proximity formula for two nuclei with a finite surface thickness[11]

$$V_{nucl} = 4\pi \bar{R} \gamma \Phi(\zeta) \quad (5)$$

The explanations of the different quantities entering in the above formula can be found in [12]. The prescission kinetic energy $TK E_{pre}$ is taken to be zero,

an assumption which proved to be reasonable for low-energy fission[5]. Also, that part of the excitation energy which is transformed into internal excitation energy E_{int}^* , is neglected. According to calculations based on time dependent quantum many-body calculations, the intrinsic excitation energy accounts for less than 15% of the collective energy gain in going from the saddle to the scission [13]. Schütte and Wilets [14] gave also an upper bound for E_{int}^* , which is still small compared to the total excitation energy E^* .

2.2 The deformation energy in the frame of the Hartree-Fock + BCS method

That part of the excitation energy which goes into the deformations of the fragments was denoted in eq.(1) by E_{def} . In the study of sf properties, E_{def} is taken usually as a sum of the liquid drop model (LDM) energy, and the shell and pairing corrections [15]. In this paper the deformation energy E_{def} of the fissioning system at scission is referred to the HF+BCS energy of the two fragments in their ground states

$$E_{def} = E_{HF+BCS}(N_1, Z_1, \beta_1) - E_{HF+BCS}(N_1, Z_1, \beta_1^{g.s.}) \\ + E_{HF+BCS}(N_2, Z_2, \beta_2) - E_{HF+BCS}(N_2, Z_2, \beta_2^{g.s.}) \quad (6)$$

Obviously this is a more general approach. The LDM, which is based on a semiclassical description of the nuclei, supplemented by the shell-effect corrective energy, is only a poore substitute for a self-consistent calculation. One of the main advantages of the self-consistent HF+BCS calculation is that it provides simultaneously both the single-particle and semiclassical properties of nuclei. The general properties of the Hartree-Fock method were reviewed in [16,17].

In our study for the HF part of the interaction we choosed the Skyrme interaction SIII [18], which succeded to reproduce satisfactory the single-particle spectra. The difference between the binding energy computed with SIII and the experimental one appears to be, for a large number of nuclei, ≈ 5 MeV [19]. It also produces a fairly well $N - Z$ dependence of the binding energy[20]. The present study envisages nuclei that are not in a closed shell configuration. Thus, the level occupations will have a large effect on the solution of the HF equations. Usually the HF method is extended to the Hartree-Fock Bogolyubov (HFB) formalism by using a mixture of different configurations in place of a single Slater determinant. However, when dealing with a Skyrme force which has been simplified such that the bulk properties of the nucleus are reproduced, one would have to introduce additional parameters in order to guarantee that sensible pairing matrix elements are obtained.

Following Vautherin [21] we assign to each orbital ϕ_k an occupation $n_k = v_k^2$,

where $u_k^2 + v_k^2 = 1$, $u_{\bar{k}} = u_k$ and $v_{\bar{k}} = -v_k$. In terms of the density $\rho(\mathbf{r}) = 2 \sum'_k n_k |\phi_k(\mathbf{r})|^2$ the HF+BCS total energy, that has to be minimized reads

$$E_{HF+BCS} = tr \left[\left(T + \frac{1}{2} \mathcal{V} \right) \rho \right] + E_p \quad (7)$$

where

$$\langle T \rangle = \frac{\hbar^2}{m} \left(1 - \frac{1}{A} \right) \sum'_k n_k \int d\mathbf{r} |\phi_k(\mathbf{r})|^2 \quad (8)$$

is the expectation value of the kinetic energy, $\mathcal{V} = tr(\rho \tilde{v})$ enters as Hartree-Fock-like potential, \tilde{v} being the antisymmetrized effective two-body interaction. The primed sum \sum' denotes a sum over all HF orbitals having projections of the total angular momentum \mathbf{j} on the z -axis $\Omega_k > 0$. To the total energy we added the pairing energy

$$E_p = -\frac{G}{4} \left\{ \sum_k \left[n_k (1 - n_k)^{\frac{1}{2}} \right] \right\}^2 \quad (9)$$

For BCS-like calculations, the matrix elements of \tilde{v} between HF states is taken to be constant

$$G = - \int d\mathbf{r} \int d\mathbf{r}' \phi_k^*(\mathbf{r}) \phi_{\bar{k}}^*(\mathbf{r}) \tilde{v}(\mathbf{r}, \mathbf{r}') \phi_l(\mathbf{r}) \phi_{\bar{l}}(\mathbf{r}) \quad (10)$$

Varying the normalized single-particle wave functions ϕ_k and their amplitudes v_k under the additional constraint $\lambda_\tau \sum_k (\delta_{\tau k, \tau} n_k - N_\tau)$, ($\tau = p, n$), ensuring that on the average the system contains the correct number of neutrons N and protons Z , we are lead to the standard HF and BCS equations [21].

The occupations n_k are determined at each step of the HF iterative calculation using the HF eigenvalues ε_k and they are employed at the next step to construct the HF field. The pairing force constant is

$$G_\tau = \frac{G_{0\tau}}{11 + N_\tau} \text{ MeV} \quad (\tau = p, n) \quad (11)$$

The constant $G_{0\tau}$ was adjusted in such a way to obtain the experimental pairing gap

$$\Delta_\tau = G \sum'_k u_k v_k \quad (12)$$

In the deformed HF calculations one have to optimize the basis which is choosen to correspond to an axial symmetric deformed harmonic-oscillator with frequencies ω_{\perp} and ω_z . Such a basis is characterized by the deformation parameter $q = \omega_{\perp}/\omega_z$ and harmonic oscillator length $b = \sqrt{m\omega_0/\hbar}$, with $\omega_0^3 = \omega_{\perp}^2\omega_z$. The basis is cut off after N_{max} major shells, where $N_{max}=10$ or 12 for the nuclei emerging in the sf of ^{252}Cf [22].

The next step consists in mapping out the potential energy curves by constraining our HF+BCS calculations in which a quadratic constraint $\frac{C}{2}(Q-Q_0)^2$ is added to the energy functional (7) [23]. Here Q_0 is a specified value of the mass quadrupole moment. In Fig.1 we represent the deformation energy curves of the nuclei ^{104}Mo and ^{148}Ba produced in the sf of ^{252}Cf .

3 Distribution of the excitation energy in the fission fragments

The scope of this section is to seek the configuration of the system at scission for a fixed excitation energy E^* . According to eq.(1), the interaction energy of two fragments with deformations β_1 and β_2 at scission is related to the excitation energy through the relation

$$V(\beta_1, \beta_2, d) = Q - E^* \quad (13)$$

where d is the tip distance and enters in the theory as a parameter. We equate this last quantity with the asymptotic kinetic energy $TKE(\infty)$. This relation is a consequence of the approximations that we made earlier, i.e. we neglected the prescission kinetic energy TKE_{pre} and we forced all the available excitation energy to be stored into deformation

$$E^*(\beta_1, \beta_2) = E_{def}(\beta_1) + E_{def}(\beta_2) \quad (14)$$

where E_{def} is computed according to eq.(7). Thus, for a given excitation energy we obtain two non-linear equations, i.e. eqs. (13) and (14).

In fig.2 we represented the excitation energy landscape (14), for the pair (^{104}Mo , ^{148}Ba). The deepest minimum corresponds to the prolate-prolate configuration (β_1, β_2) . At this point $E^* = 0$ and fission proceeds by means of only one channel, customarily known as cold fission. This configuration has deformations $\beta(^{104}\text{Mo})=0.370$ and $\beta(^{148}\text{Ba})=0.270$ which are very close to those computed in the frame of the finite-range droplet macroscopical model [24]. The non-linear equations, quoted above, admit this solution only for the tip distance $d = 2.95$ fm, a value very close to the border of 3 fm, alleged by the Tübingen group, bellow which cold fission occurs [3].

When we increase the excitation energy, an infinity of solutions arise according to eq.(14). They have to be identified with the geometrical locus of points with equal excitation energy. However, the second constraint (13) is limiting drastically the number of (β_1, β_2) pairs. In Fig. 3 we give the contour plots of the excitation energy and superposed on them the curves relating β_1 to β_2 for different tip distances. The intersection of such curves with the contour lines of equal excitation energy will give the physical solutions to our fission problem, i.e. for certain tip distance intervals, one get different scission configurations or channels.

As one observe one get generally two solutions which are located mainly for low-excitation energy in the quadrant with $\beta_1, \beta_2 > 0$. While for pure cold fission ($E^* = 0$) one get a solution only for one d , when $E^* > 0$ one get solutions for several values of d . Naturally, one may ask next if all these solutions are likely to occur. For that one should look at the ratio of excitation energies between the two fragments. Calculations based on the cascade evaporation model predicted a ratio of the mean excitation energies $E_2^*/E_1^* \approx 0.5$ around the splitting 104/148 when approaching the limiting case of cold fission [25]. According to the same reference, disproportions in sharing of the excitation energy should be expected only in the vicinity of magic numbers. For our study case we are left only with few possibilities for a given excitation energy, which are listed in Table I for $E^* = 0, 2, 4$ and 6 MeV.

In fig.4 we give the fragments density contour lines for a fixed excitation energy, namely $E^* = 2$ MeV and different tip distances.

4 Conclusions

Based on a molecular model in which the scission configuration has to fulfill two main energetic constraints, namely that the interaction between the fragments is converted totally into asymptotic kinetic energy and that the excitation energy of the fissioning system is accounted only by the deformation energy, we carried constrained HF+BCS calculations at zero temperature for the nuclei emerging in the low-energy fission reaction. For a fixed excitation energy we varied the distance between the tips of the fragments. Each case admits not more than two solutions, i.e. to pairs of fragments deformations. The criteria which allowed us to select the valid scission configuration was that of the excitation energy distribution between the fragments. We discarded those configurations with a disproportionate ratio between the excitation energies of the two fragments. A careful analyse exhibited roughly two regions of tip distance which can be assigned as valid scission configurations. The first one has the starting point at $d = 2.95$ fm and goes up to 3.8 fm whereas the second is much narrow and is centered around $d = 5$ fm. In this last case that

should be less probable to occur, one of the fragments is emitted with oblate deformations.

For excitation energies higher than those considered in this paper, the properties of the nuclear system are described by a thermal average, the influence of the shell effects becoming thus less important.

A limitation of the present approach is caused by the absence of higher multipole deformations (octupole, hexadecupole, etc.). As have been shown very recently [2], the account of hexadecupole deformation provided the explanation of a whole region of cold fission for ^{252}Cf .

Also we intend to study the fragments angular momentum formation in these fragments based on a very recent proposal of some of us [26] together with the evolution of several collective variables during the post-scission motion.

Acknowledgements One of the authors(Ş.M.) would like to acknowledge the financial support from CIES-France. He is also very indebted to N.Pilet, I.N.Mikhailov and dr.A.Florescu for fruitful discussions.

References

- [1] G.M. Ter-Akopian et al., Phys.Rev.Lett.**73** (1994) 1477.
- [2] A. Săndulescu, Ş. Mişicu, F. Carstoiu, A. Florescu and W. Greiner, Phys.Rev. C **58** (1998) 2321.
- [3] M. Crönni, A. Möller, A. Kötze, F. Gönnerwein, A. Gagarski and G. Petrov, Proceedings of the International Conference *Fission and Properties of Neutron-Rich Nuclei*, eds. J.H.Hamilton and A.V.Ramayya, p.109, World Scientific, Singapore 1998.
- [4] F.Gönnerwein and B.Borsig, Nucl.Phys.**A530**, 27(1991).
- [5] B.D.Wilkins, E.P.Steinberg and R.R.Chasman, Phys.Rev. C **14** (1976) 1832.
- [6] W.Nörenberg, Zeit.Phys. 197 (1966) 246.
W.Nörenberg, Phys.Rev. C **5** (1972) 2020.
- [7] A. Săndulescu, A. Florescu, F. Carstoiu, W. Greiner, J.H. Hamilton, A.V. Ramayya and B.R.S. Babu, Phys.Rev. C **54** (1996) 258.
- [8] U. Brosa, S. Grossmann and A. Müller, Phys.Rep. **197** (1990) 167.
- [9] S. Cohen and W.J. Swiatecki, Ann.Phys. (N.Y.) **19** (1962) 67.

- [10] P. Quentin, J. Phys. **30** (1969) 497.
- [11] J. Blocki, J. Randrup, W.J. Swiatecki and C.F. Tsang, Ann.Phys. (N.Y.) **105** (1967) 427.
- [12] Y.-J. Shi and W.J. Swiatecki, Nucl.Phys.**A464** (1987) 205.
- [13] H. Walisser, K.K. Wildermuth and F. Gönnerwein, Z.Phys. A **329** (1988) 209.
- [14] G. Schütte and L. Wilets, Nucl.Phys.A **252** (1975) 21.
- [15] K. Vanderbosch and J.R. Huizenga, *Nuclear Fission*, pag.27, Academic Press, New York (1973).
- [16] P. Quentin and H. Flocard, Ann.Rev.Nucl.Part.Sci.**28**, (1978) 523.
- [17] P. Ring and P. Schuck, *The Nuclear Many-Body Problem*, Springer, New York 1980.
- [18] M. Beiner, H. Flocard, Nguyen van Giai and P. Quentin, Nucl.Phys. A **238** (1975) 29.
- [19] P. Quentin, Thèse d'État, Université de Paris-Sud, France (1975).
- [20] N. Tajima, P.Bonche, H.Flocard, P.-H. Heenen and M.S. Weiss, Nucl.Phys. A **551** (1993) 434.
- [21] D.Vautherin, Phys.Rev. C **7** (1973) 296.
- [22] H.Flocard, P. Quentin and D.Vautherin, Phys.Lett. B **46** (1973) 304.
- [23] H.Flocard, P. Quentin, A.K.Kerman and D.Vautherin, Nucl.Phys. A **203** (1973) 433.
- [24] P. Möller, J.R. Nix, W.D. Myers and W.J. Swiatecki, At.Data Nucl. Data Tables **59** (1995) 185.
- [25] H. Märten and D. Seeliger, J.Phys. G : Nucl.Phys. **10** (1984) 349.
- [26] I.N. Mikhailov and P.Quentin, preprint CSNSM 99-01, 1999.

Figure legends

Fig.1 The deformation energy curves of the nuclei ^{148}Ba and ^{104}Mo computed in the frame of the HF+BCS method with quadratic constrain for the mass quadrupole

Fig.2 Three-dimensional plot of the excitation energy E^* for the pair (^{148}Ba , ^{104}Mo) computed in the frame of the HF+BCS method.

Fig.3 Graphical solution of the non-linear equations (13) and (14). The intersection of the solid curve with the contour lines provides two solutions in the particular case of the pair (^{148}Ba , ^{104}Mo), with tip distance $d = 3.25$ fm and total excitation energy $E^* = 2$ MeV.

Fig.4 Fragments density contour lines for excitation energy $E^*=2$ MeV and tip distances $d = 2.6, 2.95, 3.10, 3.25$

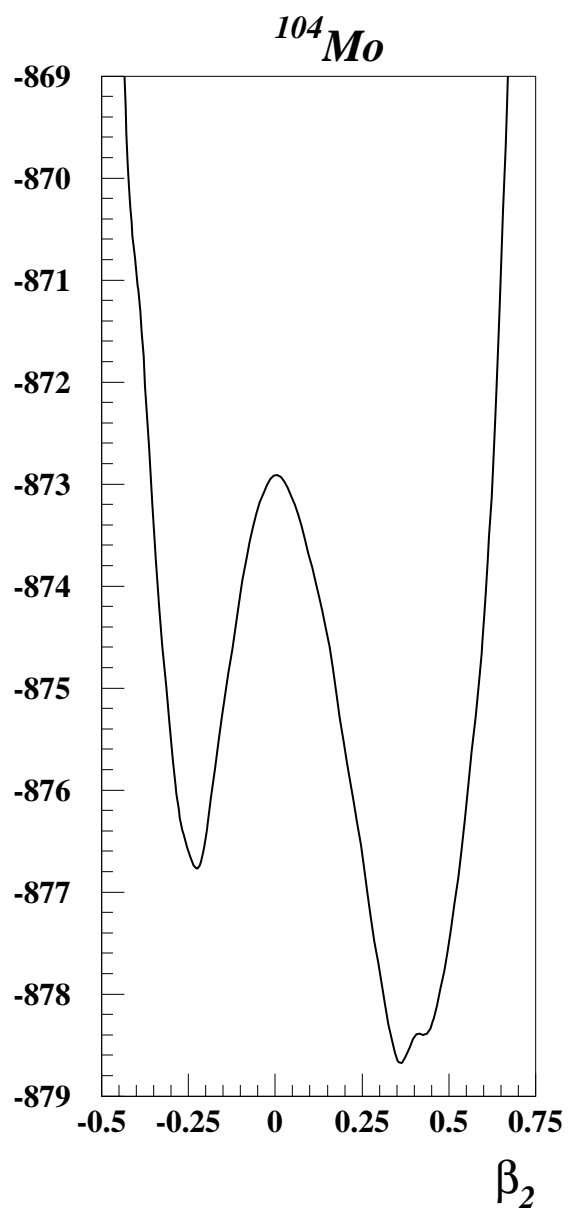
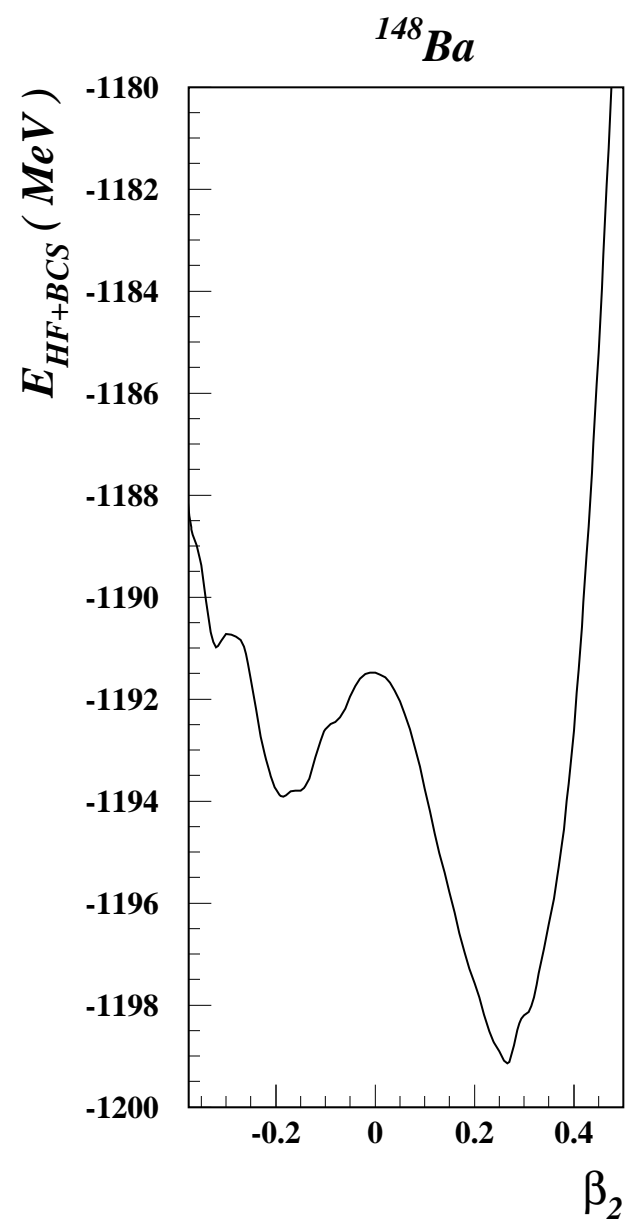
Table 1

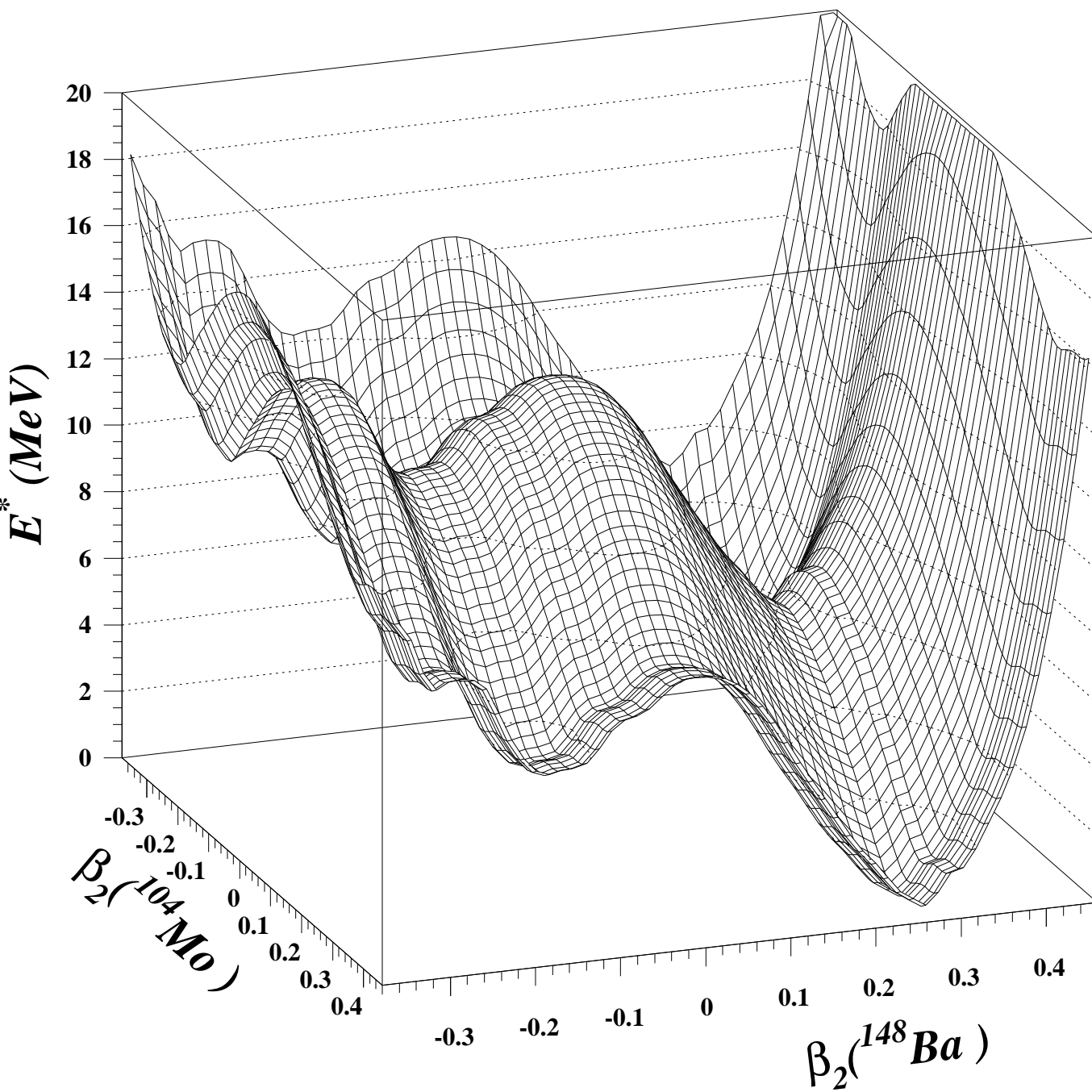
Pairs of fragments deformations (β_1, β_2) and ratio of excitations energies E_2^*/E_1^* for different excitation energies E^* and tip distances d .

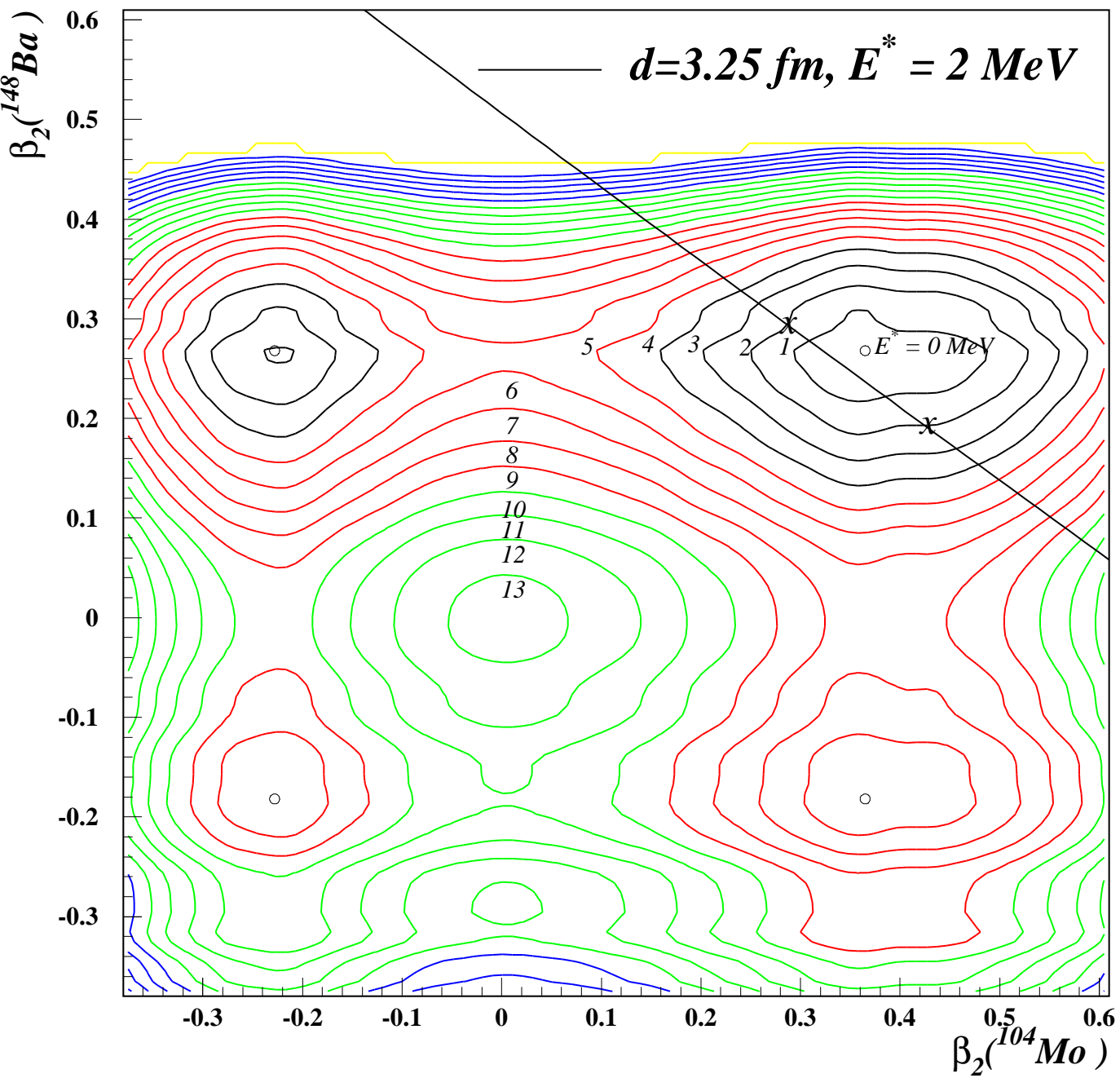
E^* (MeV)	d (fm)	β_1	β_2	E_2^*/E_1^*
0	2.95	0.270	0.370	-
2	2.60	0.313	0.492	0.94
	2.65	0.325	0.463	0.30
		0.263	0.533	260.
	2.95	0.215	0.486	0.8
		0.335	0.351	0.01
	3.00	0.209	0.475	0.5
		0.332	0.338	0.1
	3.10	0.198	0.452	0.2
		0.322	0.313	0.5
	3.15	0.194	0.438	0.2
		0.317	0.302	1.4
	3.20	0.309	0.293	1.1
4	2.60	0.342	0.520	0.70
	3.10	0.182	0.530	0.91
		0.366	0.324	0.11
	3.15	0.175	0.520	0.70
		0.362	0.311	0.20
	3.20	0.168	0.510	0.53
		0.357	0.300	0.30
	3.25	0.352	0.286	0.41
		0.162	0.499	0.40
	3.35	0.341	0.263	0.74
		0.151	0.475	0.31
	3.40	0.335	0.252	0.98
		0.146	0.463	0.14
	3.85	0.175	0.265	0.71
	4.95	0.335	-0.212	0.99
	5.00	0.337	-0.226	0.9

Table 1
(continued)

E^* (MeV)	d (fm)	β_1	β_2	E_2^*/E_1^*
6	2.75	0.447	0.409	0.46
	3.25	0.158	0.564	0.99
		0.388	0.306	0.14
3.30		0.151	0.555	0.81
		0.385	0.293	0.21
3.35		0.143	0.546	0.65
		0.381	0.279	0.28
3.40		0.134	0.535	0.51
		0.377	0.265	0.38
3.45		0.128	0.526	0.43
		0.373	0.253	0.48
3.50		0.121	0.516	0.34
		0.368	0.239	0.61
3.55		0.114	0.504	0.26
		0.364	0.226	0.73
3.60		0.108	0.493	0.20
		0.360	0.213	0.87
5.00		0.373	-0.213	0.49
5.05		0.374	-0.227	0.46
5.15		0.371	-0.250	0.52
5.20		0.370	-0.262	0.58
5.25		0.367	-0.272	0.65
5.30		0.364	-0.282	0.75
5.35		0.359	-0.291	0.90
5.40		0.353	-0.300	1.1







TXE = 2 MeV

